Applied Surface Science 394 (2017) 586–597

Contents lists available at ScienceDirect

Applied Surface Science

journal homepage: www.elsevier.com/locate/apsusc

Full Length Article

Investigation of nano-structured Zirconium oxide film on Ti6Al4V substrate to improve tribological properties prepared by PIII&D

Sehrish Saleem[a,c], R. Ahmad[a,b,*], R. Ayub[b], Uzma Ikhlaq[a], Weihong Jin[c], Paul K. Chu[c]

[a] Department of Physics, Government College University, Lahore 54000, Pakistan
[b] Centre for Advanced Studies in Physics (CASP), Government College University, Lahore 54000, Pakistan
[c] Department of Physics and Materials Science, City University of Hong Kong, Tat Chee Avenue, Kowloon, Hong Kong

ARTICLE INFO

Article history:
Received 23 November 2015
Received in revised form 9 September 2016
Accepted 19 September 2016
Available online 25 October 2016

Keywords:
PIII&D
Zirconium oxide
Wear
XPS
Nanoindentation

ABSTRACT

Plasma immersion ion implantation and deposition (PIII&D) is the most attractive and efficient technique used in the medical field to tailor materials for biomedical applications. In the present study zirconium oxide nano-structured thin films were deposited on surface of Ti6Al4V alloy for bias voltages of 15, 20 and 25 kV. The chemical composition, surface roughness and thickness of deposited films were characterized by the x-ray photoelectron spectroscopy (XPS), atomic force microscope (AFM) and ellipsometry respectively. The XPS results confirm the formation of a dense zirconium oxide film of the treated specimens. AFM results exhibit a smooth film with maximum roughness of about 8.4 nm is formed. The thickness of the film is increased with the increase in bias voltages and is maximum at 25 kV. The effect of bias voltages on wear characteristics was further investigated by pin-on-disk test. It is observed that the friction coefficient is reduced, whereas wear resistance is enhanced and it is found to be maximum at 25 kV compared to the other bias voltages. Nanohardness is improved up to twice compared to untreated specimen at the maximum bias voltage. Therefore, it is concluded that deposition of zirconium oxide using the PIII&D is produced a dense layer on the substrate surface, which can be used as a promising candidate for the improved tribological properties of Ti6Al4V.

1. Introduction

The demand of biomaterials in various applications such as dental roots, stents, joint replacements and orthopedic fixation has been increased in recent era. It is difficult and time-consuming to design new biomaterials and therefore the most economical way is to modify surface properties of existing biomaterials to fulfill the modern requirements [1–3]. The surface of implanted material can be altered using thin film deposition techniques. Different deposition techniques have appeared in the available literature. However among these, plasma immersion ion implantation and deposition (PIII&D) is becoming the versatile technique to modify the surface properties of the materials over the last decade [4–6]. PIII&D has the potential to alter the surface properties of without any change in bulk [5]. Moreover, ions can be incorporated into the materials approximately up to the depth of hundreds of nanometer using PIII&D which has been widely used in the medical field to improve the bio-medical properties of polymers, metals and there alloys [5–7].

Ti6Al4V alloy is the most suitable material for biomedical implants as compared to the pure Ti and some of its other alloys due to its high mechanical strength, modulus of elasticity comparable to the bone, good biocompatibility and excellent corrosion resistance [8,9]. However, Ti6Al4V alloy exhibits the poor tribological properties, limiting its use in load-bearing applications [10,11]. Liang et al. [12] reported that degradation of artificial implants like knee, elbow and hip joints were occurred after 10–15 years of use. The main causes behind this degradation were wear failures. Moreover, it was observed that wear particles promoted the corrosion process resulting in genetic damage [13]. Therefore, it is imperative to make these implant materials wear and corrosion resistant. The wear resistance of implant material can be enriched by improving the hardness of substrate to inhibit defections and ploughing due to counter load [14]. This can be achieved by coating the different materials on the surface of Ti and its alloy.

* Corresponding author at: Department of Physics, Government College University, Lahore 54000, Pakistan.
E-mail address: ahriaz@gcu.edu.pk (R. Ahmad).

http://dx.doi.org/10.1016/j.apsusc.2016.09.091
0169-4332/

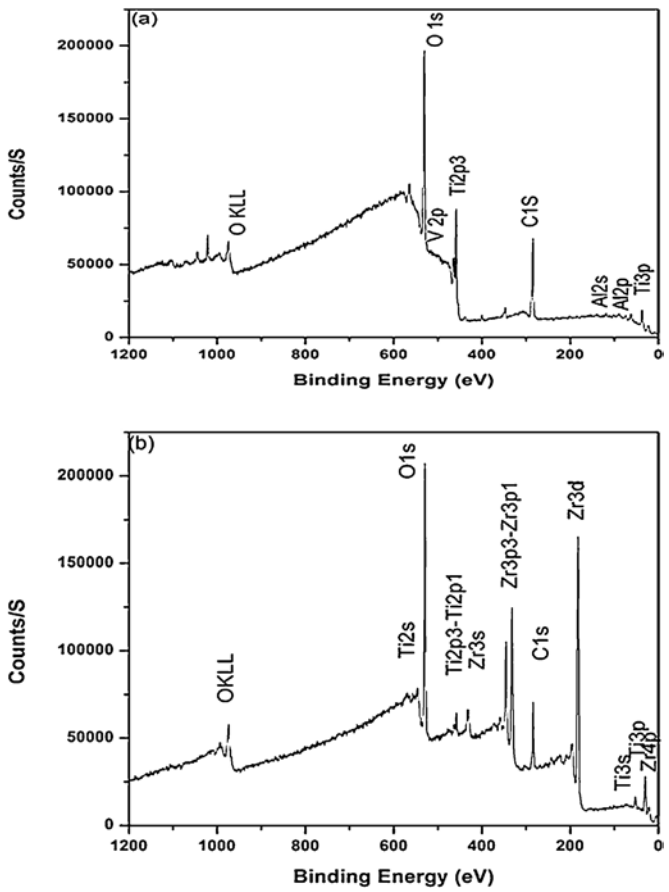

Fig. 1. Survey Scan spectrum of (a) untreated Ti6Al4V (b) ZrO_2 deposited specimen.

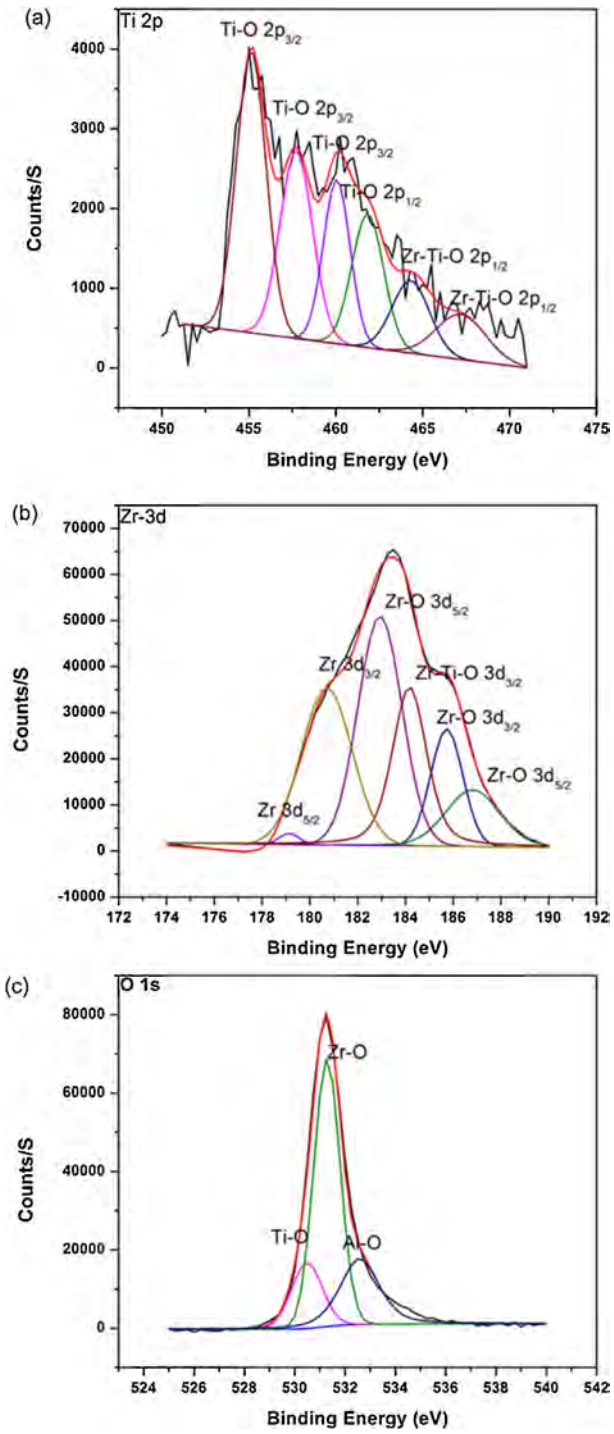

Fig. 2. Deconvoluted XPS spectrum of (a) Ti 2p (b) Zr 3d (c) O1s.

Ganapathy et al. [8] deposited the Al_2O_3 and 8mole% of Yttrium-stabilized ZrO_2 composite coating on Ti6Al4V which exhibited a superior wear resistance. The wear rate was found to be 253 times lower as compared to the Ti6Al4V alloy. The decrease in wear rate was due to the formation of dense structure, improving the hardness of the substrate. Similarly, Narvaez et al. [14] observed the wear mechanism of TiAlN coating at different bias voltages and concluded that the film grown at −40 V exhibited the best tribological properties. In another study Obadele et al. [15] coated Ti6Al4V with ZrO_2 in Ti matrix and observed decrease in the friction coefficient with enhanced wear resistance. More recently, Liu et al. [16] observed that the friction coefficient of texture surface decreased after the nitrogen ion implantation improving the wear resistance was improved. Although many researchers have made the considerable efforts to improve the wear behavior of Ti6Al4V alloy but to the best of our knowledge, no one has prepared the nano-structured zirconium oxide film at various voltages by PIII&D technique. Therefore the aim of present study is to explore the effect of nano-structured zirconium oxide film on tribological properties of Ti6Al4V alloy.

2. Experimental details

Ti6Al4V samples (10 mm × 10 mm × 2 mm) were mechanically grinded to mirror polished with SiC papers grit (200-1200), ultrasonically rinsed in acetone, ethanol and distilled water (10 min each) and then dried in air before its exposure to plasma. Plasma immersion ion implantation and deposition (PIII&D) was carried out in the plasma ion implanter housed in plasma laboratory, City University of Hong Kong. The details of PIII equipment and implanter are mentioned elsewhere [17]. The base pressure of 1.3×10^{-2} Pa was achieved in the vacuum chamber by mechanical and turbo molecular pumps. Argon gas was used for cleaning the specimens by means of sputtering. Zirconium cathode was used to produce zirconium ions to deposit Zirconium oxide thin film. High purity argon (Ar 99.99% pure) and oxygen (O_2 99.99% pure) gases were fed into the chamber to generate the plasma at 30 sccm and

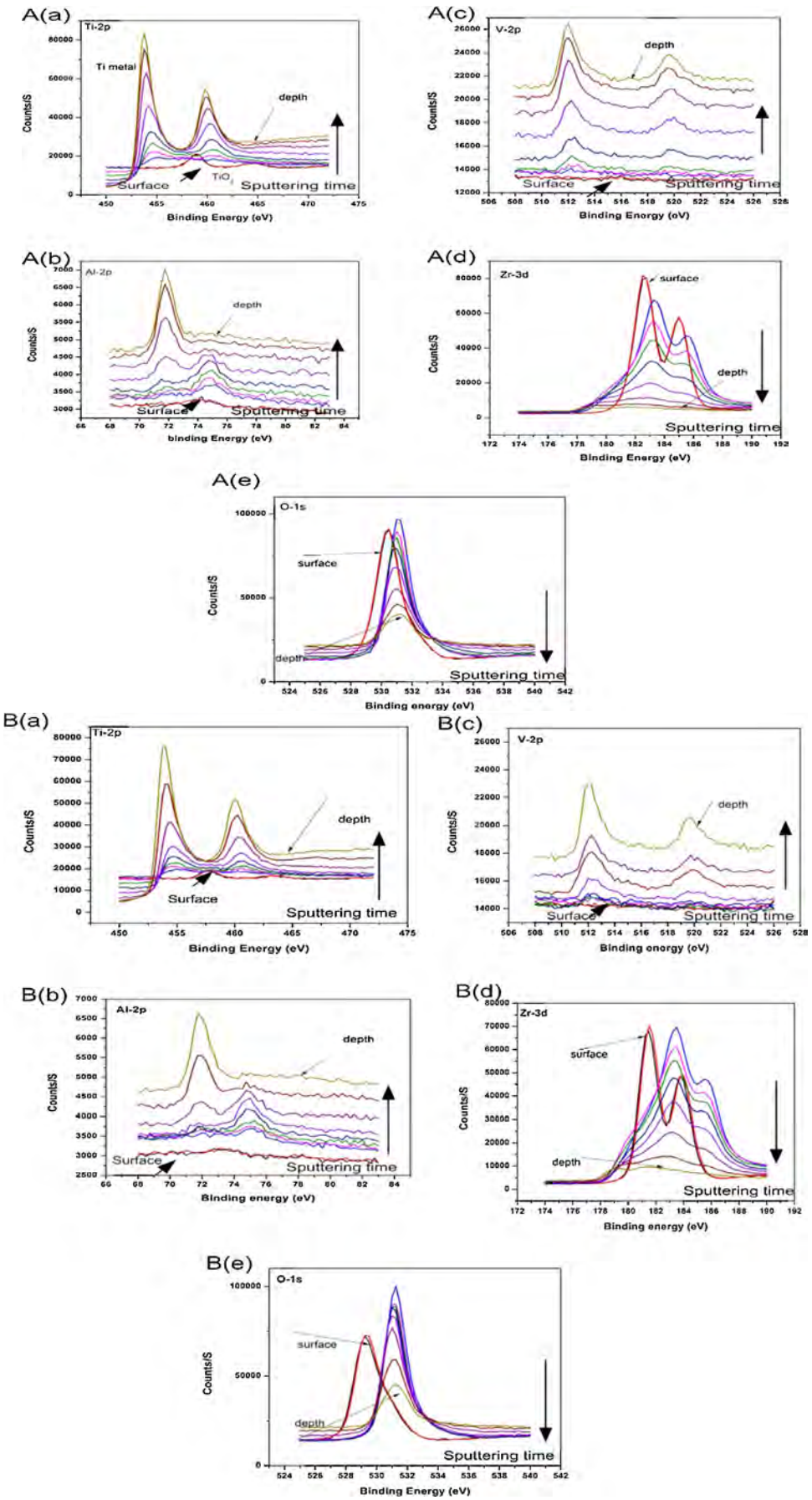

Fig. 3. Detail X-ray photoelectron spectroscopy (XPS) spectra of (a) Ti 2p, (b) Al 2p, (c) V 2p, (d) Zr 3d, (e) O1s, Each individual graph consist of ten different spectrum after successive Ar sputtering, (A-Series) specimens treated at 15 kV, (B-series) at 20 kV, (C-series) at 25 kV.

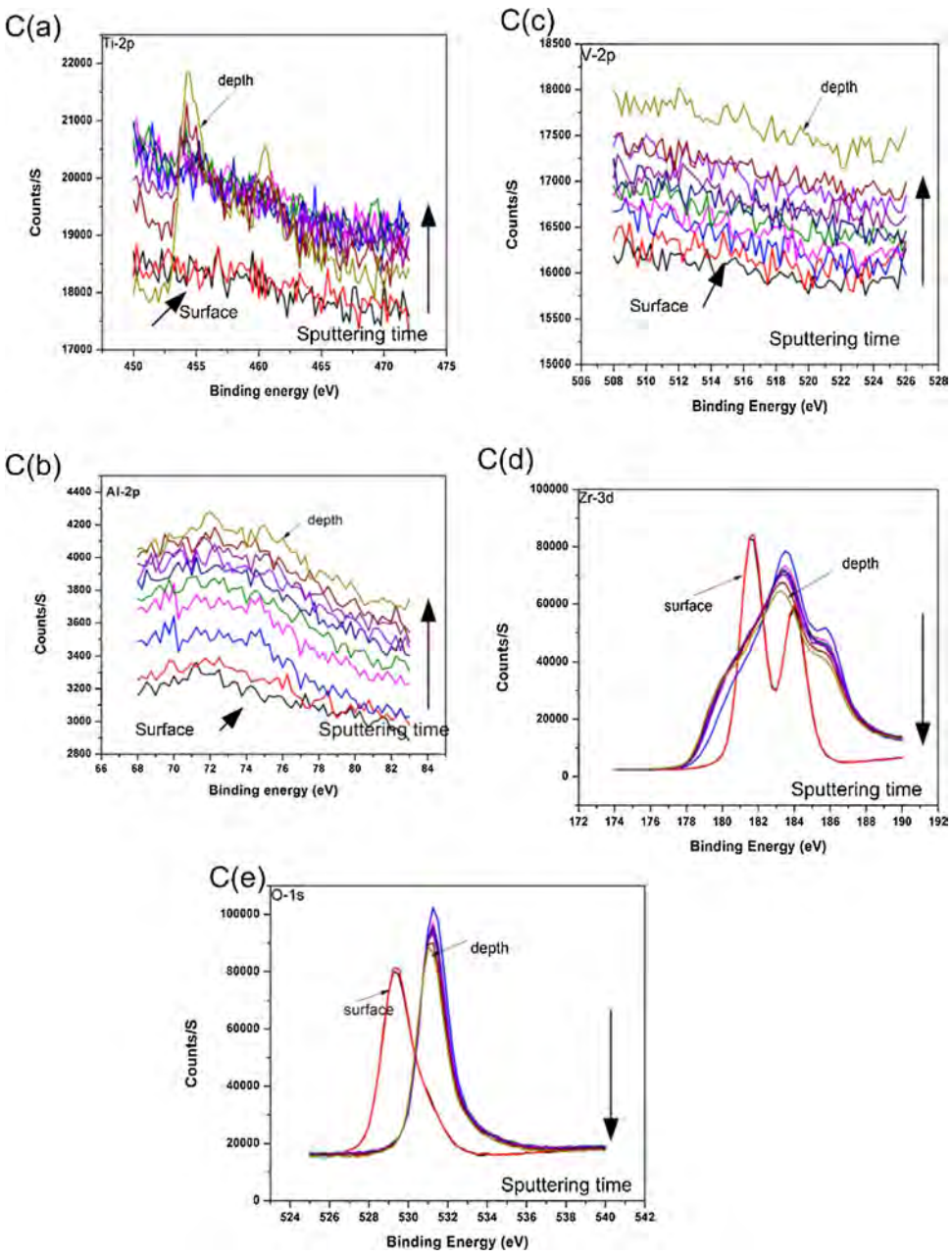

Fig. 3. (*Continued*)

20 sccm respectively. The specimens were treated at three different voltages of 15 kV, 20 kV and 30 kV for 120 min treatment time.

The chemical compositions of the outermost layer of the films were determined by X-ray photoelectron spectroscopy (XPS) (PHI Model 5802) at a base pressure of 10^{-8} Torr using AlK_{α} X-ray (1486.6 eV). A Gaussian peak fitting model was adopted to deconvolute the spectra using Casa XPSPEAK41 software. Argon ion beam was used to sputter off deposited film upto 50 nm depth to investigate the elemental analysis. The dry sliding wear tests were performed using a pin-on disk machine (TEER Coating Ltd., Model POD-2). A standard WC ball with a diameter of 5 mm was used. The tests were conducted at a constant sliding speed of 300 mms^{-1} under loads of 2 and 7 N. Atomic force microscopy (AFM, Park Scientific Instruments) was used to determine the surface topography and roughness of the specimens surface before and after deposition. Thickness of films was measured using ellipsometery (Alpha-SE). The scanning electron microscopy (SEM, JEOL JSM-820) was utilized to examine the surface morphology of the specimens. The hardness (H) was determined by nano-indentation (MTS Nano Indenter XP, USA).

3. Results and discussion

3.1. X-ray photoelectron spectroscopy (XPS)

In the present study, untreated and treated specimens at 15, 20 and 25 kV were analyzed using X-ray photoelectron spectroscopy (XPS). Survey scan spectra of untreated and treated specimens over a binding energy range from 0 to 1200 eV are shown in Fig. 1(a–b). The peaks of untreated spectrum are assigned as Ti 2p, Al (2p, 2s),

and V 2p. The presence of C1s in untreated spectrum indicating surface contamination from the atmosphere and the peak at 976 eV correspond to the Auger peak of OKLL, which is due to the oxidation of specimens [18]. The spectrum of deposited specimen in Fig. 1(b) clearly reveals the presence of significant peaks of zirconium (Zr 3s, Zr 3p, Zr 3d and Zr 4p) along with oxygen (O 1s).

For the identification and confirmation the presence of different compounds/phases, high-resolution spectra for Ti 2p over binding energy ranging from 450 eV to 470 eV, while for Zr 3d (175 eV–190 eV) and for O1s (525–540 eV) are plotted. The deconvolution of these plots was done using Casa XPS Peak41 software and results are shown in Fig. 2(a–c). In Fig. 2(a), four peaks are assigned to titanium oxide at binding energies of 455.1, 457.6, 460.1 and 461.8 eV, whereas two peaks show bonding between Ti—Zr—O at binding energy (BE) values of 464.3 and 467.2 eV. Similarly the deconvolution of Zr 3d peak (Fig. 2(b)) also show the presence of Zr—O bonding at BE values 186.7, 185.73 and 182.9 eV and Zr—Ti—O bonding at BE values of 184.15 eV. Furthermore, the existence of Zr $3d_{5/2}$ and Zr $3d_{1/2}$ is also observed at low BE values of 179.13 eV and high BE value 181.7 eVrespectively, as depicted in Fig. 2(b). The deconvoluted spectrum of O1s (Fig. 2(c)) only highlights the presence of bonding of metal oxides which are Zr—O at BE of 531.2 eV, Ti—O at BE of 532.6 eV and Al—O at BE of 530.4 eV. All the deconvoluted peaks are matched by the standard data of NIST web site [19].

In Fig. 3(A–C) is shown the variation of XPS spectra of deposited films as a function of sputter time for different voltages (15 kV, 20 kV and 25 kV). For all the spectra plotted in Fig. 3, sputter rate selected for 50 nm depth was 6.955 nm/min. It is evident from the Ti2p spectra (Fig. 3A (a)), that peaks of titanium are gradually improved with depth. This means that less amount of titanium has been observed at the surface but with the gradual increase in depth, the amount of titanium is enhanced. Also significant chemical shifting towards higher binding energy depicts the titanium oxidation states confirming the existence of titanium dioxide (Ti^{4+}) on the surface of specimen whereas pure metal (Ti) is found at a lower binding energy. The atoms of a higher positive oxidation state exhibit a higher binding energy due to the extra coulomb interaction between the photo-emitted electron and the ion core. In Al 2p and V 2p spectra as shown in Fig. 3. A (b) and A (c), a similar behavior of peaks is found i.e, the peaks of vanadium and aluminum become significant with the increasing depth. On the other hand in case of Zr 3d and O 1s spectra (Fig. 3A (d) and A (e)), the maximum amount of zirconium and oxygen was present at the top surface of specimen which is gradually decreased with the increasing depth. This also confirms the formation of zirconium oxide film at 15 kV.

The spectra of treated specimen corresponding to 20 kV as shown in Fig. 3(B-series) exhibit almost similar results as depicted in A-series. However, the variation in spectrum of specimen treated at 25 kV (C-series) exhibits different results showing a better deposition at higher voltage as compared to the films prepared at relatively lower voltage. The results reveal that the peaks related to Ti 2p, Al 2p and V 2p are not prominent at surface whereas the spectra corresponding to Zr 3d and O1s show strong peaks not only on the top of surface but also at some deeper region. It is also interesting to note here that zirconium peaks exist even at 50 nm with significant intensity exhibiting the formation of a thick film as compared to the films at low voltages. Additionally shifting of peaks at different depths of the samples shows the formation of various compounds in oxygen 1s spectrum.

The variation in atomic concentration of different elements as a function of Ar sputter time is shown in Fig. 4(a–c). The results indicate that atomic concentrations crossponding to Ti 2p, Al 2p and V 2p are increased with the sputtering time whereas in case of Zr 3d and O 1s atomic concentrations are decreased as given in Fig. 4(a & b). By comparison of Fig. 4(a) and (b), apparently no noticeable

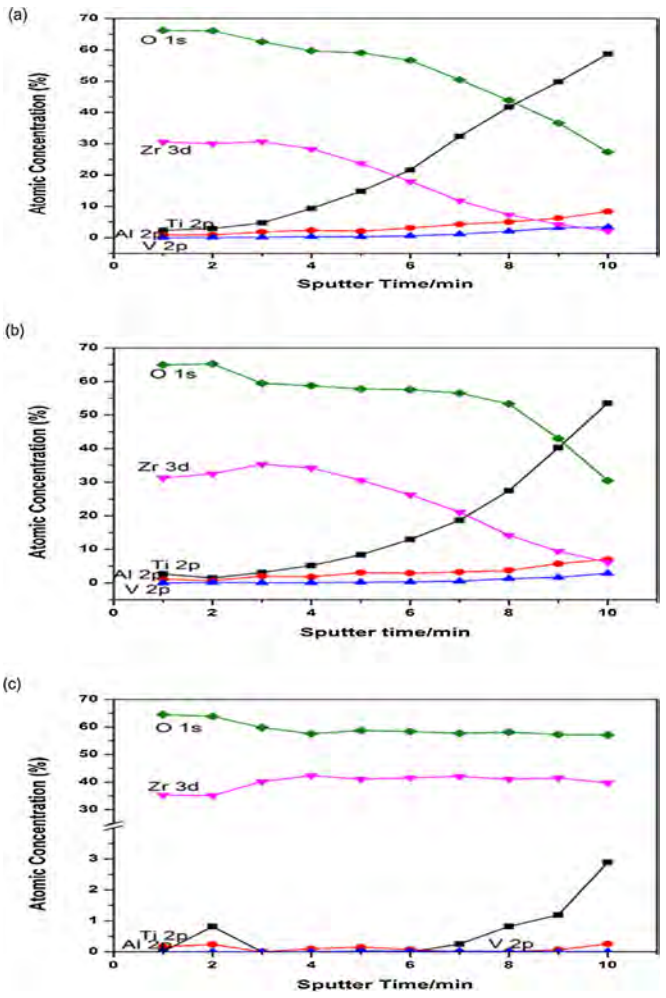

Fig. 4. Graphical representation of Atomic concentration versus sputter time (a) 15 kV (b) 20 kV (c) 25 kV.

Table 1
Roughness values of deposited film by AFM analysis.

	R_q nm	R_a nm	R_z nm
Untreated	1.58	1.26	1.15
15 kV	2.51	1.94	0.535
20 kV	7.64	6.41	7.20
25 kV	8.45	7.02	1.55

difference is observed for the specimens treated at 15 and 20 kV. On the other hand the specimen treated at 25 kV (Fig. 4(c)) show that Zr 3d and O 1s remain stable on the surface even after sputtering, whereas presence of V 2p and Al 2p is found to be insignificant. These results indicate that thicker film has been formed at 25 kV, which might be due to a better diffusion of Zr and O at higher voltage as compared to the specimen treated at lower voltage.

3.2. AFM

The surface morphology of the treated and untreated specimens has been investigated using the Atomic force microscopy (AFM) and is given in Fig. 5(a–d). The roughness values, R_a (average roughness), R_q (root mean square (RMS)) and R_z (ten-point mean height) are mentioned in Table 1. These values were calculated by taking the average of three different areas. The 3-D micrograph

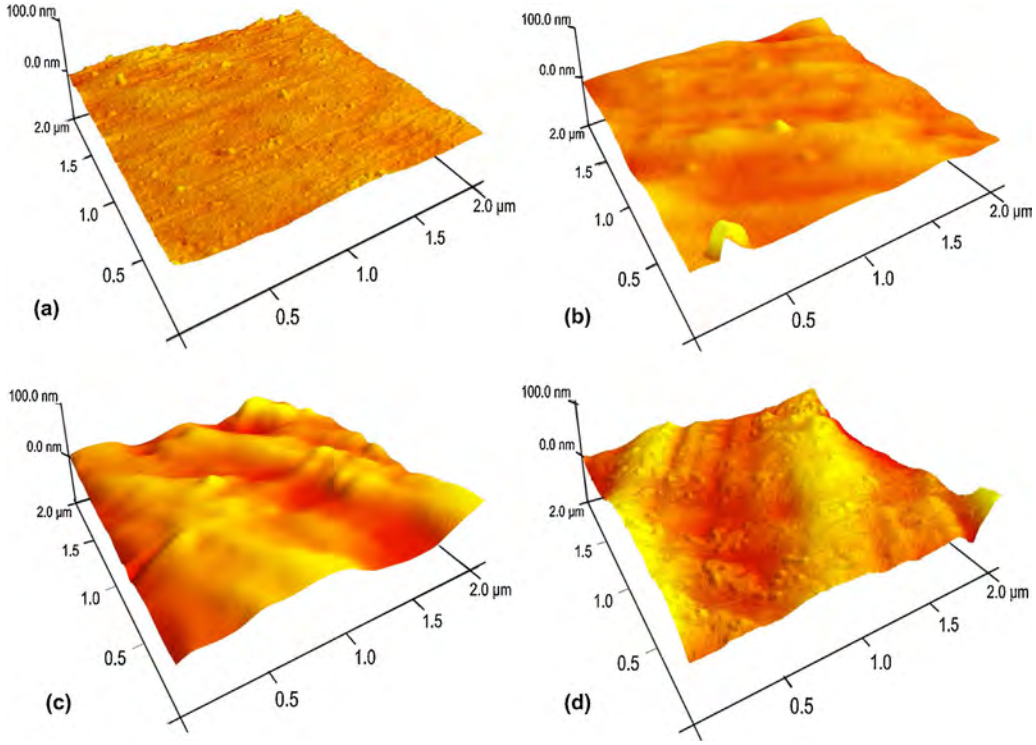

Fig. 5. AFM micrographs of deposited film (a) untreated (b) 15 kV (c) 20 kV (d) 25 kV.

of untreated specimen has shown minor scratches on the surface which might have produced during the polishing (Fig. 5(a)). On the other hand, the surface of treated specimens at 15 kV and 20 kV (Fig. 5(b–c)) depicted some hillocks formation; as a result the roughness has been increased. Surface morphology of specimen at 25 kV is quite different showing waves like patterns/structures all over the area. It is found that the surface roughness of all the treated specimens increased with the rise in voltages. The maximum roughness has been achieved at 25 kV which is about 8.45 nm. The AFM results are also confirmed the formation of nano structured film on the substrate. The increase in surface roughness relates to the growth mechanism which is influenced by both the sputtering and deposition effects [20]. Since, with the increase in bias voltages, sputter and deposition rate are increased resulting in the formation of a thick layer with high roughness [21].

3.3. Thickness

The average thickness of deposited films was measured at three different areas using the ellipsometry (incident angle 70°). The influence of bias voltages on thickness of deposited films is given in Fig. 6. The average thickness is found to be approximately 60, 83 and 108 nm for bias voltages 15, 20 and 25 kV respectively. Thickness increases linearly with the bias voltages which is in agreement with the results reported by Wu et al. [22].

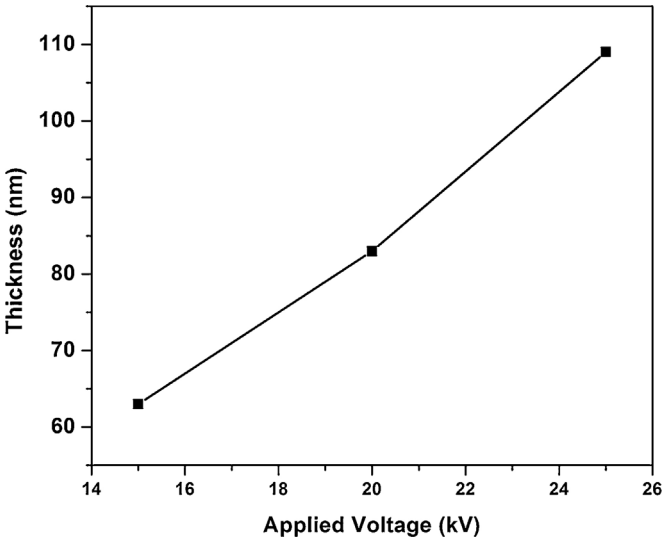

Fig. 6. Variation in thickness at different voltages.

3.4. Wear results

The instrument used to study the wear resistance is a conventional pin-on-disk system. The pin was mounted on a stiff lever and loaded onto the sample (in the form of a disk) with a precisely known weight. During the wear test, the specimens were rotated against a stationary tungsten carbide (WC) ball of 5 mm diameter at a linear velocity of 300 mm/min for 2000 number of cycles. All the tests were conducted in air and without lubrication at normal loads of 2 N and 7 N. As the disk was rotated, the resulting frictional force acting between the pin and disk was measured from the small lateral deflections of the lever. The wear coefficients for the material pair were calculated from the volume of material lost after a specific number of revolutions. The wear rate W (mm^3/N-m) of the deposited film was calculated by the given relationship [23].

$$W = \frac{V}{D \times P}$$

Where V (mm^3) is a volume of the removed particles (debris), P (N) is the normal applied load and d (m) is the total distance.

The resultant wear track left on the specimens was analyzed using a surface profilometer in order to accurately determine the

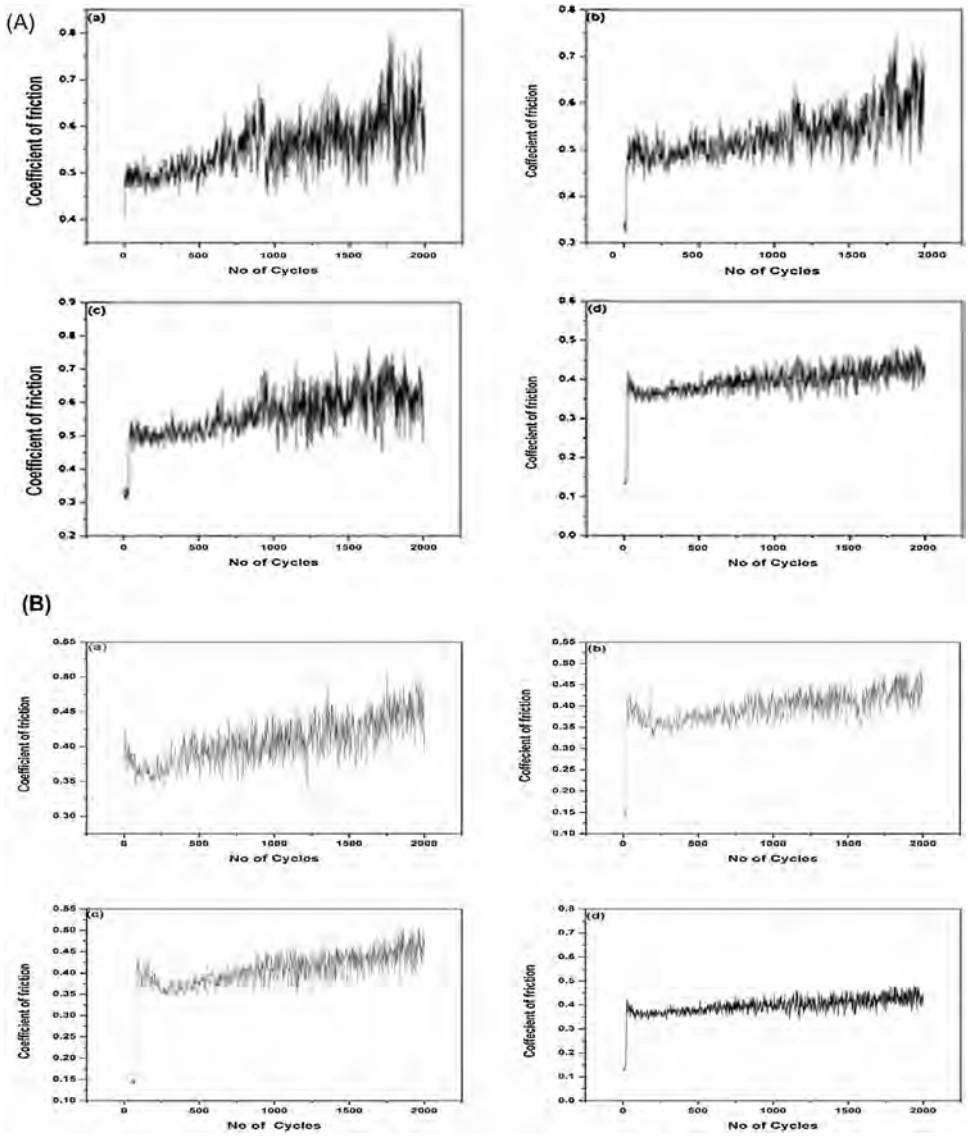

Fig. 7. Friction Coefficient as a function of no of cycles. (A) at 2 N (B) at 7 N (a) untreated, (b) 15 kV, (c) 20 kV, (d) 25 kV.

Table 2
Min. and Max. of coefficient of friction.

	Min-Max at 2 N	Min-Max at 7 N
Untreated	0.42–0.8	0.3–0.51
15 k eV	0.32–0.75	0.14–0.51
20 k eV	0.31–0.77	0.14–0.51
25 k eV	0.13–0.49	0.13–0.49

depth. The variations in coefficient of friction (COF) of untreated and treated specimens as a function of sliding cycles (2000) against tungsten carbide (WC) balls are given in Fig. 7(A–B). Initial COF of the untreated specimen is ~0.42 at load of 2 N and reaches its maximum value ~0.8, whereas at 7 N load COF varies from ~0.3 to 0.5. The minimum and maximum values of COF against the 2 N and 7 N loads are presented in Table 2. It is clear from the table values that for 2 N load COF was decreased in all the treated specimens. Moreover, for 2 N load significant decrease in COF is observed at 25 kV. In addition, COF initially drops for 7 N load (Fig. 7(B)) and then becomes stable as compared to the untreated specimen.

Fig. 8(a–b) reveal the influence of voltages on wear rate of untreated and deposited specimens at 2 N and 7 N loads. These results show that for 2 N load, wear rate is continuously decreased in all the deposited specimens with the rise in the bias voltages as given in Fig. 8(a). The same trend (Fig. 8(b)) has been observed in case of 7 N load. However, the decrease in wear rate is more significant at 25 kV for both loads as compared to the other voltages. The results also revealed that the COF also reduced at 25 kV. The prominent variation in both wear rate and COF at the 25 kV is due to the formation of dense zirconium oxide layer on the substrate surface which is also supported by the XPS depth profile results, where zirconium oxide remains present on the surface as compared to the other treated specimens. Moreover, the thickness of the deposited film is higher at 25 kV as compared to the other voltages, which is in agreement with the literature [22,24,25].

To achieve better understanding, the data regarding wear tracks obtained using a surface texture tester is given in Fig. 9(A–B). In the

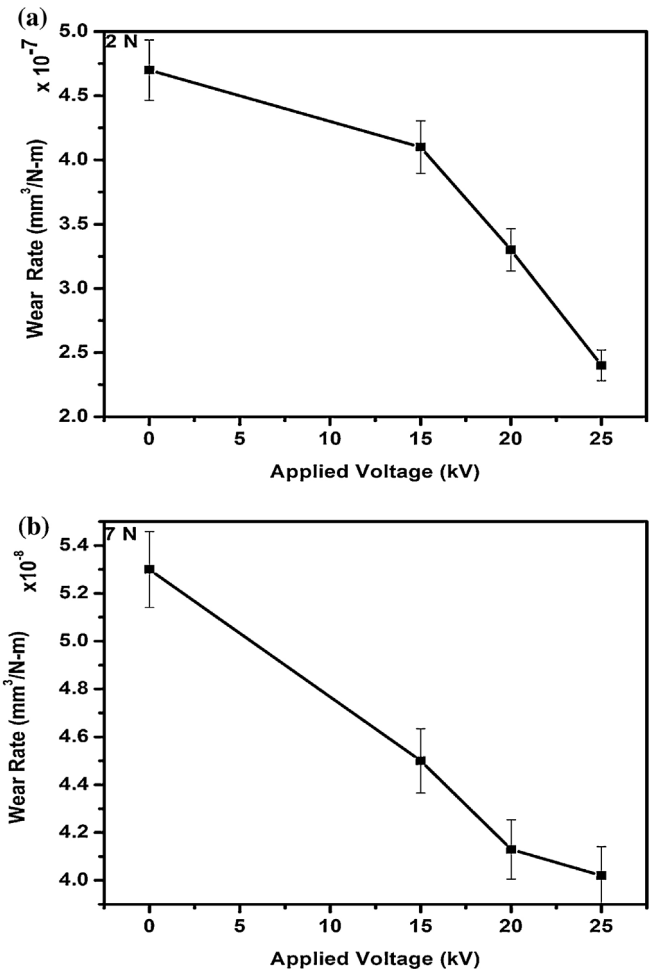

Fig. 8. Variation of wear rates with applied voltages at (a) 2 N (b) 7 N load.

wear mechanism, a material is removed from surface of the solid. The amount of the removed material can be estimated with the help of wear profile. The wear depth relates the removed material at the given point of the contact area. The wear profile is a function of the wear depth with respect to position at the contact region. The variation in depth and area of grooves of the untreated and treated samples are shown in Fig. 10(a–b). The depths of these grooves are of the order of few micrometers. A graphical representation of these grooves is shown in Fig. 10(a–b). Untreated specimen exhibits a deep and wide wear groove, whereas the implanted specimens display narrow and relatively compact grooves. The improvement and compactness of these grooves are caused by surface hardening due to ion implantation [26]. The decrease in wear track width indicates better tribological properties [22].

SEM microstructure of worn out surfaces of untreated and treated specimens after the wear track at loads 2 N and 7 N are shown in Figs. 11 (a–d) & 12 (a–d) respectively for 500× magnifications. Fig. 11(a) shows SEM micrograph of untreated specimen exhibiting rough surface that reveals adhesive wear behavior because many adhesive craters and grooves are observed after wear ploughing. On the other hand the surface of treated specimens is almost same except the film deposited at 25 kV which indicates relatively less surface worn, when the counterpart slides as shown in Fig. 11(d). The main reason of good wear resistance at 25 KV is due to its low COF and presence of thick zirconium oxide layer on the top of the surface. It is desirable to have high wear resistance (less debris from the surface) for bio-implant. On the other hand, micrographs of untreated specimen at 7 N load (Fig. 12(a)) show spallation, whereas micrograph of treated specimens at 15 KV and 20 KV are almost similar, which has indicated a relatively better morphology than untreated. But asperities on the surface are deformed and worn out which showing poor adhesion of film to the substrate. Wear tracks of specimen deposited at 25 kV show better morphology as compared to specimens treated at lower voltages.

3.5. Nanohardness measurements

The mechanical behavior was investigated by nanoindentation using a nanoindenter (Nano Instruments XP, MTS) with the continuous stiffness measurement (CSM) capability. The indentation was carried out using a Berkovich (three-sided pyramid) indenter. The indentation experiments were conducted in displacement control to a depth range upto 200 nm on each specimen to measure the film properties as shown in Fig. 13. It is observed from the figure that with the increase in depth, hardness decreased near the film substrate interface and becomes stable at other places. It has been reported by many researchers [27–29] that hardness increased with the decrease in depth which is due to thickness effect. Since, the maximum thickness of implanted specimens is found to be 108 nm. Therefore, beyond the 100 nm depth hardness

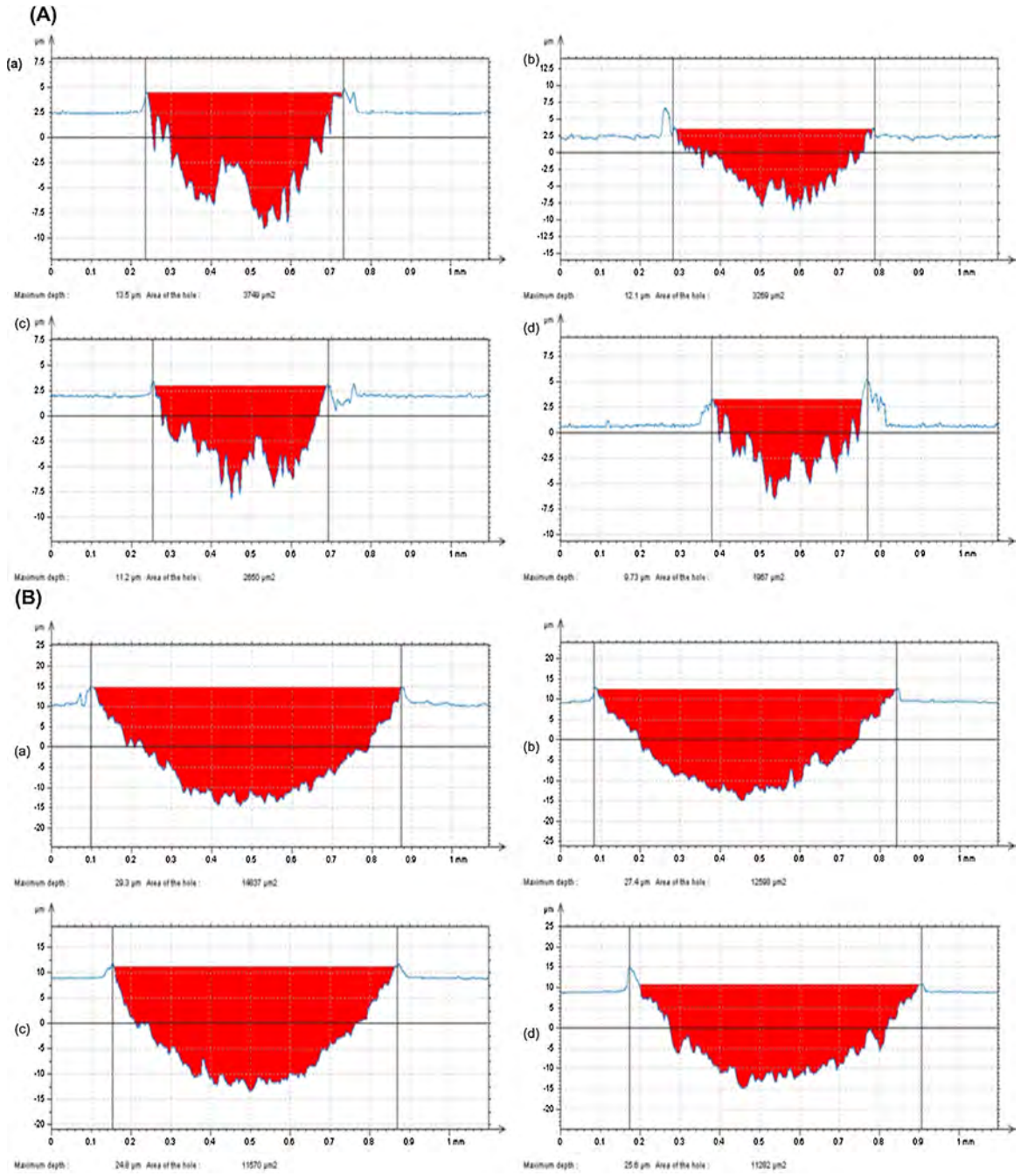

Fig. 9. Depth profiles of wear track as a function of different voltages (A) 2 N, (B) 7 N, (a) untreated, (b) 15 kV, (c) 20 kV, (d) 25 kV.

results are due to the deposited layer as well as the bulk substrate [30].

The influence of bias voltage on hardness of treated and untreated specimens is given in Fig. 14. The hardness was measured by taking the average of indentations at three different areas. It is clear from the graph that hardness of all treated specimens has higher as compared to the untreated specimen. The surface hardness is found to vary from 5.5 GPa to 10.5 GPa, which is about 2 times as compared to untreated specimen. Moreover, it is observed that with an increase in the bias voltage the hardness also increased, which is supported by earlier studies [31–37]. Since with an increase in voltages, more energetic ions bombard on the substrate surface, as resulted more compact and dense zirconium oxide film is formed with improved hardness.

4. Conclusions

The present work addressed the study of tribological behavior of nano-structured zirconium oxide films prepared by using PIII&D system at various applied voltages on Ti6Al4V substrate. XPS depth profile results reveal the formation of dense nano-zirconium oxide film at 25 kV because of the presence of sharp peaks of Zr-3d even after the Ar sputtering of surface for 8 min. Surface roughness and thickness are increased in bias voltages. Whereas, friction coeffi-

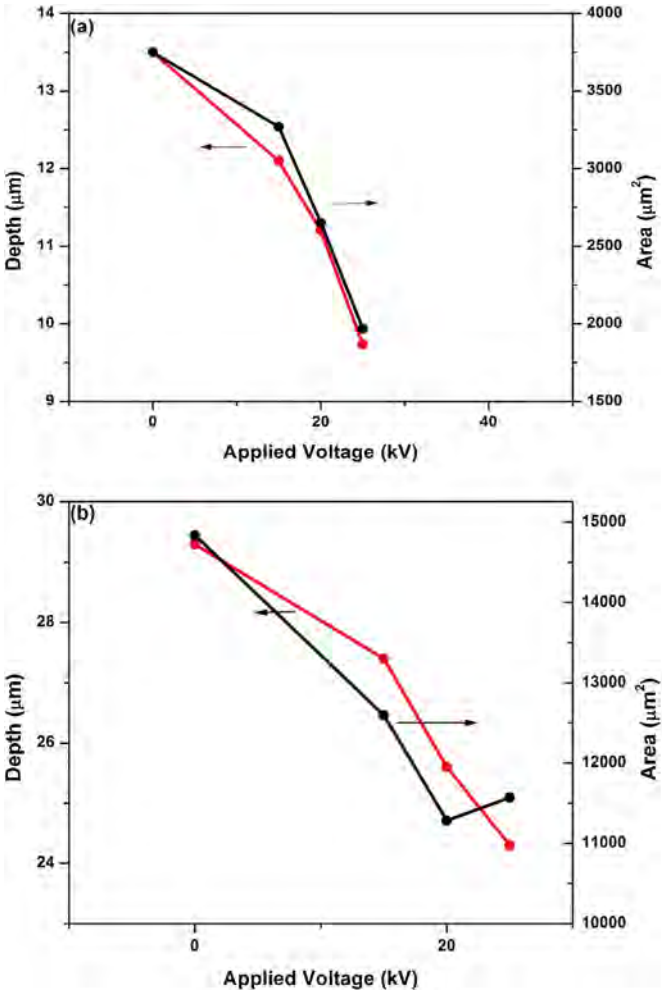

Fig. 10. Variation in depth and area of grooves at different applied voltages, (a) 2 N (b) 7 N.

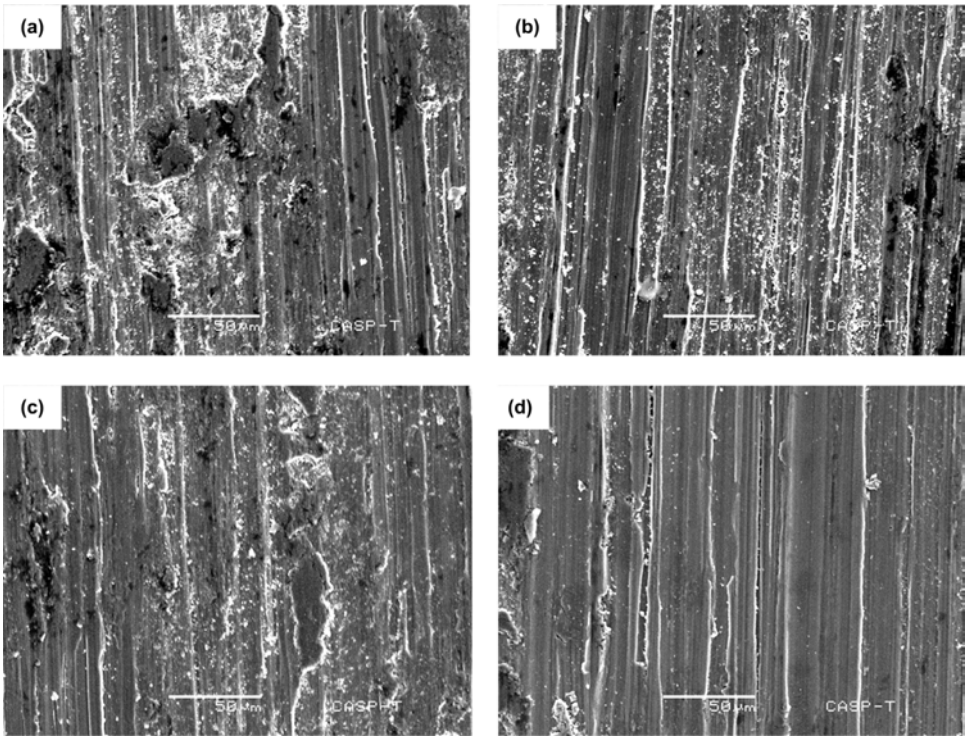

Fig. 11. SEM micrographs of wear track of untreated and treated specimens at 2 N load (a) untreated (b) 15 kV, (c) 20 kV, (d) 25 kV.

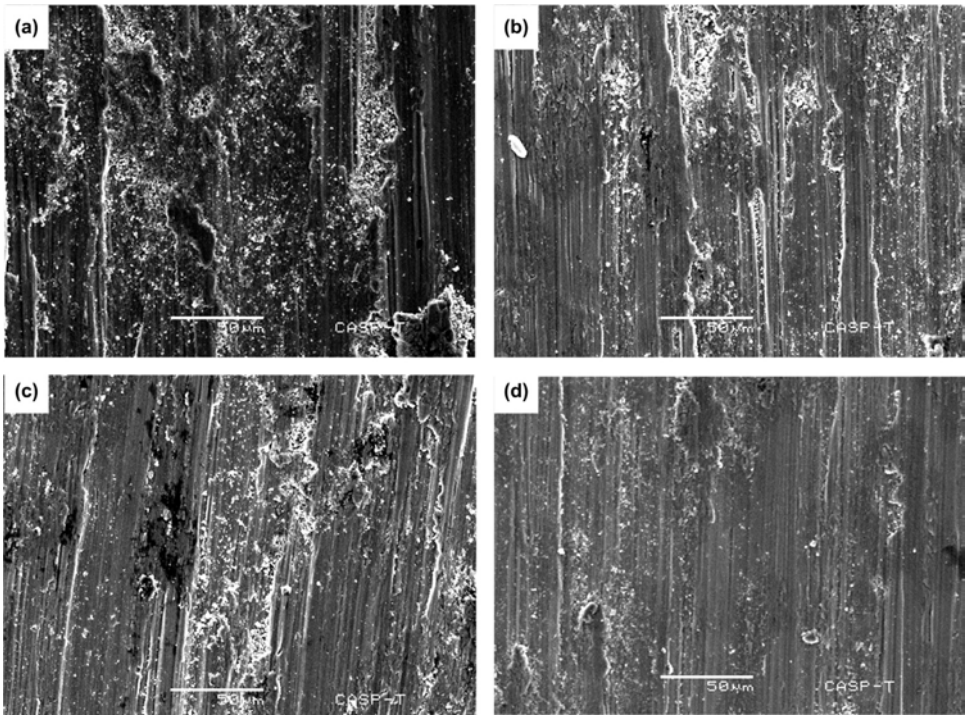

Fig. 12. SEM micrographs of wear track of untreated and treated specimens at 7 N load (a) untreated (b) 15 kV, (c) 20 kV, (d) 25 kV.

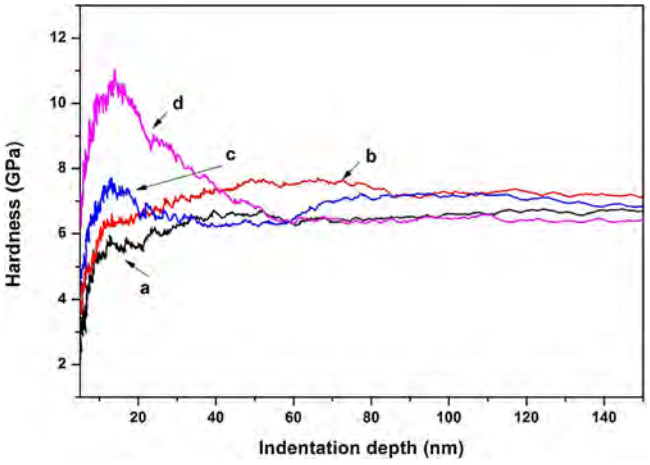

Fig. 13. Nanohardness as a function of indentation depth (a) untreated (b) 15 kV, (c) 20 kV, (d) 25 kV.

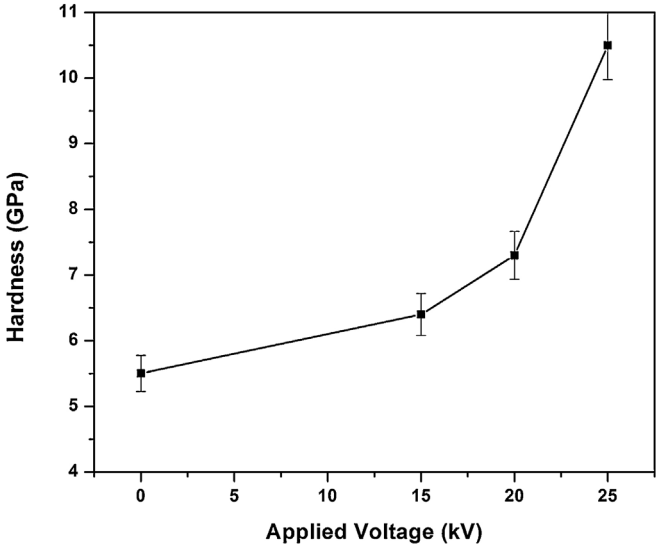

Fig. 14. Surface hardness as a function of applied voltage.

cient and wear rate of zirconium oxide deposited specimens are found to be lower than the untreated specimen. However, hardness of all treated specimens is found to be higher. Moreover, the wear resistance and hardness has improved with rise in bias voltage. It is concluded that deposition of zirconium oxide at 25 kV produces a dense layer on substrate surface which significantly has improved the tribological properties of Ti6Al4V alloy.

Acknowledgments

The authors are grateful to Higher Education Commission Pakistan for providing scholarship under IRSIP and Hong Kong Research Grants Council (RGC) and City University of Hong Kong Applied Research Grant (ARG). Authors are also grateful to Mr. Wang Chen-Xi and other members of the Plasma Laboratory of City University of Hong Kong for experimental assistance. We are also thankful to Dr. Tousif Hussain (CASP), Dr. Ahmad Zafari (The University of Melbourne) and S. Lau for valuable help for SEM and wear analysis and AFM analysis.

References

[1] Y. Zhao, K.W.K. Yeung, P.K. Chu, Functionalization of biomedical materials using plasma and related technologies, Appl. Surf. Sci. 310 (2014) 11–18.
[2] G. Wu, J.M. Ibrahim, P.K. Chu, Surface design of biodegradable magnesium alloys—a review, Surf. Coat. Technol. 233 (2013) 2–12.
[3] T. Lu, Y. Qiao, X. Liu, Surface modification of biomaterials using plasma immersion ion implantation and deposition, Interface Focus 2 (2012) 325–336.
[4] H. Feng, G. Wang, G. Wu, W. Jin, H. Wu, P.K. Chu, Plasma and ion-beam modification of metallic biomaterials for improved anti-bacterial properties, Surf. Coat. Technol. (2016), http://dx.doi.org/10.1016/j.surfcoat.2016.05.059 (in press).

[5] P.K. Chu, J.Y. Chen, L.P. Wang, N. Huang, Plasma-surface modification of biomaterials, Mater. Sci. Eng. R 36 (2002) 143–206.
[6] Y. Zhao, S.M. Wong, H.M. Wong, S. Wu, T. Hu, K.W.K. Yeung, P.K. Chu, Effect of carbon and nitrogen plasma immersion ion implantation on in vitro and in vivo biocompatibility of titanium alloy, Appl. Mater. Interfaces 5 (2013) 1510–1516.
[7] R. Xu, X. Yang, X. Zhang, M. Wang, P. Li, Y. Zhao, G. Wu, P.K. Chu, Effects of carbon dioxide plasma immersion ion implantation on the electrochemical properties of AZ31 magnesium alloy in physiological environment, Appl. Surf. Sci. 286 (2013) 257–260.
[8] P. Ganapathy, G. Manivasagam, A. Rajamanickam, A. Natarajan, Wear studies on plasma-sprayed Al_2O_3 and 8mole% of yttrium-stabilized ZrO_2 composite coating on biomedical Ti-6Al-4 V alloy for orthopedic joint application, Int. J. Nanomed. 10 (2015) 213–222.
[9] M. Long, H.J. Rack, Titanium alloys in total joint replacement-a materials science perspective, Biomaterials 19 (1998) 1621–1639.
[10] Y.M. Wang, B.L. Jiang, L.X. Guo, T.Q. Lei, Tribological behavior of micro arc oxidation coatings formed on titanium alloys against steel in dry and solid lubrication sliding, Appl. Surf. Sci. 252 (2005) 2989–2998.
[11] M. Masmoudi, M. Assoul, M. Wery, R. Abdelhedi, F. El Halouani, G. Monteil, Friction and wear behavior of cp Ti and Ti6Al4V following nitric acid passivation, Appl. Surf. Sci. 253 (2006) 2237–2243.
[12] H. Liang, B. Shi, A. Fairchild, T. Cale, Applications of plasma coatings in artificial joints: an overview, Vacuum 73 (2004) 317–326.
[13] B. Daley, A.T. Doherty, B. Fairman, C.P. Case, Wear debris from hip or knee replacements causes chromosomal damage in human cells in tissue culture, J. Bone Jt. Surg. 86 (2004) 598–606.
[14] D.M.D. Narvaez, J.M.V. Restrepo, E.R. Parra, Bias voltage influence on the mechanical and tribological properties of titanium aluminum nitride coatings produced by triode magnetron sputtering, Revista Materia 20 (2015) 115–126.
[15] B.A. Obadele, A. Andrews, P.A. Olubambi, M.T. Mathew, S. Pityana, Effect of ZrO2 addition on the dry sliding wear behavior of laser clad Ti6Al4V alloy, Wear 328–329 (2015) 295–300.
[16] D. Liu, Q. Zhang, Z. Qin, Q. Luo, Z. Wu, L. Liu, Tribological performance of surfaces enhanced by texturing and nitrogen implantation, Appl. Surf. Sci. 363 (2016) 161–167.
[17] E.C. Rangel, P.A.F. Silva, R.P. Mota, W.H. Schreiner, N.C. Cruz, Thin polymer films prepared by plasma immersion ion implantation and deposition, Thin Solid Films 73 (2) (2005) 259–266.
[18] Y. Cheng, Y.F. Zheng, Surface characterization and mechanical property of TiN/Ti-coated NiTi alloy by PIIID, Surf. Coat. Technol. 201 (15) (2007) 6869–6873.
[19] http://srdata.nist.gov/xps/main_search_menu.aspx.
[20] C.F. Huang, H.C. Cheng, C.M. Liu, C.C. Chen, K.L. Ou, Microstructure and phase transition of biocompatible titanium oxide film on titanium by plasma discharging, J. Alloys Compd. 476 (2009) 683–688.
[21] C. Ottone, M. Laurenti, K. Bejtka, A. Sanginario, V. Cauda, The effects of the film thickness and roughness in the anodization process of very thin aluminum films, J. Mater. Sci. Nanotechnol. 1 (1) (2014) 1–9.
[22] Z. Wua, X. Tian, Z. Wang, C. Gong, S. Yang, C.M. Tan, P.K. Chu, Microstructure and mechanical properties of CrN films fabricated by high power pulsed magnetron discharge plasma immersion ion implantation and deposition, Appl. Surf. Sci. 258 (2011) 242–246.
[23] J. Nohava, P. Dessarzin, P. Karvankova, M. Morstein, Characterization of tribological behavior and wear mechanisms of novel oxynitride PVD coatings designed for applications at high temperatures, Tribol. Int. 81 (2015) 231–239.
[24] L. Wang, X. Hu, X. Nie, Deposition and properties of zirconia coatings on a zirconium alloy produced by pulsed dc plasma electrolytic oxidation, Surf. Coat. Technol. 221 (2013) 150–157.
[25] E. Zdravecka, V.M. Tiainen, Y.T. Konttinen, L. Franta, M. Vojs, M. Marton, M. Ondac, J. Tkacova, Relationships between the fretting wear behavior and mechanical properties of thin carbon films, Vacuum 86 (2012) 675–680.
[26] F. Jin, P.K. Chu, Z. Xu, J. Zhao, M. Zhu, R.K.Y. Fu, H. Tong, Surface modification of W9Cr4V2Mo high-temperature bearing steel by rare earth ion implantation, Surf. Coat. Technol. 201 (2006) 4357–4360.
[27] M. Berg, C.V. Budtz-Jorgensen, H. Reitz, K.O. Schweitz, J. Chevalliier, P. Kringhoj, J. Bottiger, On plasma nitriding of steels, Surf. Coat. Technol. 124 (2000) 25–31.
[28] H.J. Spies, B. Reinhold, K. Wilsdorf, Surf. Eng. 17 (1) (2001) 41–54.
[29] Z.A. Umar, R.S. Rawat, K.S. Tan, A.K. Kumar, R. Ahmad, T. Hussain, C. Kloc, Z. Chen, L. Shen, Z. Zhang, Hard TiCx/SiC/a-C:H nanocomposite thin films using pulsed high energy density plasma focus device, Nucl. Instrum. Methods Phys. Res. B 301 (2013) 53–61.
[30] Y. Liu, L. Li, M. Xu, X. Cai, Q. Chen, Y. Hu, P.K. Chu, Effects of nitrogen ion implantation and implantation energy on surface properties and adhesion strength of TiN films deposited on aluminum by magnetron sputtering, Mater. Sci. Eng. A 415 (2006) 140–144.
[31] N. Dwivedi, S. Kumar, H.K. Malik, Studies of pure and nitrogen-incorporated hydrogenated amorphous carbon thin films and their possible application for amorphous silicon, J. Appl. Phys. 111 (2012) 014908-1––014908-16.
[32] N. Dwivedi, S. Kumar, H.K. Malik, Strange hardness characteristic of hydrogenated diamond-like carbon thin film by plasma enhanced chemical vapor deposition process, Appl. Phys. Lett. 102 (2013) 011917.
[33] N. Dwivedi, S. Kumar, H.K. Malik, Superhard behavior, low residual stress, and unique structure in diamond-like carbon films by simple bilayer approach, J. Appl. Phys. 112 (2012) 023518.
[34] N. Dwivedi, S. Kumar, H.K. Malik, Role of ex-situ oxygen plasma treatments on the mechanical and optical properties of diamond-like carbon thin films, Mater. Chem. Phys. 134 (2012) 7–12.
[35] N. Dwivedi, S. Kumar, H.K. Malik, C.M.S. Govind, O.S. Rauthan, Panwar Correlation of sp3 and sp2 fraction of carbon with electrical, optical and nano-mechanical properties of argon-diluted diamond-like carbon films, Appl. Surf. Sci. 257 (2011) 6804–6810.
[36] N. Dwivedi, S. Kumar, H.K. Malik, Nanoindentation measurements on modified diamond-like carbon thin films, Appl. Surf. Sci. 257 (2011) 9953–9959.
[37] N. Dwivedi, S. Kumar, J.D. Carey, H.K. Malik, Govind, Photoconductivity and characterization of nitrogen incorporated hydrogenated amorphous carbon thin films, J. Appl. Phys. 112 (2012) 113706.